Theoretical examination of quantum coherence in a photosynthetic system at physiological temperature

Akihito Ishizaki[a,b] and Graham R. Fleming[a,b,1]

[a]Department of Chemistry, University of California, Berkeley, CA 94720; and [b]Physical Bioscience Division, Lawrence Berkeley National Laboratory, Berkeley, CA 94720

Contributed by Graham R. Fleming, August 7, 2009 (sent for review June 4, 2009)

The observation of long-lived electronic coherence in a photosynthetic pigment–protein complex, the Fenna–Matthews–Olson (FMO) complex, is suggestive that quantum coherence might play a significant role in achieving the remarkable efficiency of photosynthetic electronic energy transfer (EET), although the data were acquired at cryogenic temperature [Engel GS, et al. (2007) Evidence for wavelike energy transfer through quantum coherence in photosynthetic systems. *Nature* 446:782–786]. In this paper, the spatial and temporal dynamics of EET through the FMO complex at physiological temperature are investigated theoretically. The numerical results reveal that quantum wave-like motion persists for several hundred femtoseconds even at physiological temperature, and suggest that the FMO complex may work as a rectifier for unidirectional energy flow from the peripheral light-harvesting antenna to the reaction center complex by taking advantage of quantum coherence and the energy landscape of pigments tuned by the protein scaffold. A potential role of quantum coherence is to overcome local energetic traps and aid efficient trapping of electronic energy by the pigments facing the reaction center complex.

photosynthesis | electronic energy transfer | quantum dynamics

Photosynthesis starts with the absorption of a photon of sunlight by one of the light-harvesting pigments, followed by transfer of the energy to the reaction center, where the primary electron transfer reactions convert the solar energy into an electrochemical gradient. (1) The transfer of this excitation energy towards the reaction center (RC) occurs with a near unity quantum yield.

The Fenna–Matthews–Olson (FMO) pigment–protein complex (2–5) is found in low light-adapted green sulfur bacteria. Under physiological conditions, this complex is situated between the so-called base-plate protein of the large peripheral chlorosome antenna and the RC complex, and is tasked with transporting sunlight energy harvested in the chlorosome to the RC pigments. The complex is a trimer made of identical subunits, each of which contains seven bacteriochlorophyll (BChl) molecules. By virtue of its relatively small size, it represents an important model in photosynthetic excitation energy transfer (EET), and has been extensively studied experimentally and theoretically. In the late 90s, Savikhin et al. (6) observed quantum beating in the FMO complex using fluorescence anisotropy technique although it had been generally assumed that electronic coherence decay so rapidly that it does not affect the EET. (7) However, it was difficult to unambiguously assign this experimental observation to an electronic origin. Recently, Engel et al. (8) investigated the FMO complex isolated from *Chlorobaculum tepidum* by means of 2D electronic spectroscopy, (9–11) and succeeded in observing long-lasting quantum beating providing direct evidence for long-lived electronic coherence. (12, 13) The observed coherence lasts for time scales similar to the EET timescales, implying that electronic excitations move coherently through the FMO protein rather than by incoherent hopping motion. Observation of long-lasting quantum coherence is not unique to the FMO complex. Lee et al. (14) revealed coherent dynamics in the RC of a purple bacteria, *Rhodobacter sphaeroides*, by applying two-color electronic coherent photon echo technique. These observations have led to the suggestion that quantum coherence might play significant roles in achieving remarkable efficiency of photosynthetic EET. Although the observations of long-lasting quantum coherence provide valuable insights into the inner working of photosynthetic complexes, the measurements were performed outside the physiological range of temperatures. Generally, quantum coherence at physiological temperatures is fragile compared to that at cryogenic temperatures because amplitude of environmental fluctuations increases with increasing temperature. Hence, the robustness and roles of quantum coherence under physiological conditions are to a large extent unknown. In order to explore these questions, theoretical investigations with models of appropriate sophistication are required in addition to further experimental studies (15–18). Recently, Aspuru-Guzik and coworkers (19–21), and Plenio and Huelga (22) discussed effects of quantum coherence on enhancement of photosynthetic EET efficiency from the perspective of a quantum walk.

Photosynthetic EET processes are usually analyzed in two perturbative limits. When the electronic coupling between pigments is small in comparison to the electron-environment coupling, which can be specified by magnitude of reorganization energy, the electronic coupling can be treated perturbatively. This treatment yields Förster theory (23), which describes incoherent hopping between pigments. In the opposite limit, when the reorganization energies are small, it is possible to treat the electron-environment coupling perturbatively to obtain a quantum master equation. The most commonly used theory from this approach in the literature of photosynthetic EET is the conventional Redfield equation (24), which is one of the few viable paths to explore quantum coherence. However, in a typical photosynthetic EET system the reorganization energies are not small in comparison to the electronic coupling. In the FMO complex, the electronic coupling strengths span a wide range, $1 \approx 100\,\mathrm{cm}^{-1}$ while the suggested reorganization energies span a similar range (11, 25–27). Hence, the Redfield equation approach might lead to erroneous insights or incorrect conclusions regarding the quantum coherence and its interplay with the protein environment (17, 18). Recently, the present authors developed a quantum dynamics equation for EET (18) by taking into account effects of the environmental reorganization dynamics on the pigments in a nonperturbative fashion based on the hierarchical expansion technique (28). The developed equation can describe EET processes irrespective of the electron-environment coupling strength, and reduces to the conventional Redfield and Förster theories in their respective limits of validity. In the regime of coherent wave-like motion, moreover, the equation predicts several times longer lifetimes of the electronic coherence between pigments than does the Redfield equation.

Author contributions: G.F. and A.I. designed research; A.I. performed research; and G.F. and A.I. wrote the paper.

The authors declare no conflict of interest.

See Commentary on page 17247.

[1]To whom correspondence should be addressed. E-mail: grfleming@lbl.gov.

This article contains supporting information online at www.pnas.org/cgi/content/full/0908989106/DCSupplemental.

In this article, we apply the aforementioned quantum dynamic equation in order to investigate the robustness and roles of quantum coherence in the *C. tepidum* FMO complex under physiological conditions. Here, special attention is paid to the EET dynamics in the site basis in order to obtain insights into the spatial and temporal evolution of electronic excitation energy through the FMO complex. Calculations are performed on the basis of the electron-environment coupling parameters adopted for simultaneous fitting of linear and 2D rephasing, nonrephasing and polarization-dependent electronic spectra (27). The numerical results reveal that electronic coherence persists for several hundred femtoseconds even at physiological temperature, $T = 300\,\mathrm{K}$. Based on the numerical results, the physical roles of quantum coherence under physiological conditions are discussed.

Theory

To describe EET dynamics in a photosynthetic complex containing N pigments, each pigment is modeled by a two-level system describing its $S_0 \rightarrow S_1$ transition (the Q_y transition of a BChl). The total Hamiltonian of the EET dynamics consists of three parts,

$$\hat{H}_{\mathrm{tot}} = \hat{H}_e + \hat{H}^{\mathrm{ph}} + \hat{H}^{\mathrm{el-ph}}. \qquad [1]$$

The first part $\hat{H}_e$ is the Hamiltonian of electronic states of the pigments expressed as

$$\hat{H}_e = \sum_{j=1}^{N} |j\rangle \varepsilon_j \langle j| + \sum_{k \neq j} |j\rangle J_{jk} \langle k|, \qquad [2]$$

where $|j\rangle$ represents the state where only the jth pigment is in its S_1 state and all others are in their S_0 states. ε_j is the so-called site energy of the jth pigment defined as the optical transition energy at the equilibrium configuration of environmental phonons associated with the S_0 state. J_{jk} denotes the electronic coupling between the jth and kth pigments. The second term $\hat{H}^{\mathrm{ph}}$ is the Hamiltonian of the environmental phonons, where the ξth mode dynamics is described by the dimensionless coordinate, $\hat{q}_\xi$. The last Hamiltonian $\hat{H}^{\mathrm{el-ph}}$ is responsible for fluctuations in the site energies by the phonon dynamics, and is expressed as

$$\hat{H}^{\mathrm{el-ph}} = \sum_{j=1}^{N} \hat{V}_j \hat{u}_j \qquad [3]$$

where we have defined $\hat{V}_j \equiv |j\rangle\langle j|$ and $\hat{u}_j \equiv -\sum_\xi c_{j\xi}\hat{q}_\xi$ with $c_{j\xi}$ being the coupling constant between the jth pigment and ξth phonon mode. The fluctuations in site energies of different pigments may be correlated or uncorrelated, depending on whether the site energies couple to the same or to different phonon modes of the protein environment. At present, however, there is no direct way to access accurate information on the correlated fluctuations in the FMO complex; hence, we assume uncorrelated fluctuations in this work.

An adequate description of the EET dynamics is given by the reduced density operator $\hat{\rho}(t) \equiv \mathrm{Tr}_{\mathrm{ph}}\{\hat{\rho}^{\mathrm{tot}}(t)\}$, where $\hat{\rho}^{\mathrm{tot}}(t)$ denotes the density operator for the total system. For the reduction we suppose that the total system at the initial time, $t = 0$, is in the factorized product state of the form, $\hat{\rho}^{\mathrm{tot}}(0) \propto \hat{\rho}(0)\exp(-\beta\hat{H}^{\mathrm{ph}})$ with $\beta \equiv 1/k_{\mathrm{B}}T$. Generally, this initial condition is unphysical since it neglects an inherent correlation between a system and its environment (28, 29). In electronic excitation processes, however, this initial condition is appropriate because it corresponds to excitation in accordance to the vertical Franck–Condon transition (18).

The coupling of an electronic transition of the jth pigment to the environmental phonons can be specified by the spectral density of the electron-phonon coupling constants, $\mathcal{J}_j(\omega)$. This includes information contents on dynamics of the environmental phonons. The equilibrium phonon state in the S_0 state is generally a nonequilibrium state in the S_1 state because of the electron-phonon coupling. After the excitation, hence, the coupling relaxes the phonons toward the actual equilibrium with dissipating the reorganization energy. The reorganization dynamics, in principle, can be measured by fluorescence Stokes shift experiment (30), where the observable quantity is the phonon relaxation function,

$$\Gamma_j(t) = \frac{2}{\pi}\int_0^\infty d\omega \frac{\mathcal{J}_j(\omega)}{\omega}\cos\omega t. \qquad [4]$$

Note that $\Gamma_j(0) \equiv 2\lambda_j$ is the Stokes shift magnitude expressed as two times the reorganization energy λ_j. Simultaneously, the coupling induces fluctuations in the site energies of pigments. Information on the timescale of the processes can be obtained by means of three-pulse photon-echo peak shift experiment (30), where the observable quantity is the phonon symmetrized correlation function, $S_j(t)$. If the environmental phonons can be described classically, the relaxation function and the symmetrized correlation function satisfy the classical fluctuation-dissipation relation, $\Gamma_j(t) = \beta S_j(t)$; hence, these two functions contain the same information on the phonon dynamics, whose characteristic timescale is given by ref. 31

$$\tau_c = \frac{1}{\Gamma_j(0)}\int_0^\infty dt\,\Gamma_j(t). \qquad [5]$$

Generally, the relaxation function has a complicated form involving several components (30). In this article, we model the relaxation function by an exponential form, $\Gamma_j(t) = 2\lambda_j\exp(-\gamma_j t)$, in order to focus on the timescale of the phonon relaxation dynamics. For this modeling, the timescale of the phonon relaxation is simply $\tau_c = \gamma_j^{-1}$, and the spectral density is expressed as the overdamped Brownian oscillator model, $\mathcal{J}_j(\omega) = 2\lambda_j\gamma_j\omega/(\omega^2 + \gamma_j^2)$. Although this spectral density has been successfully used for analyses of experimental results (27, 32, 33), it may produce qualitatively different phonon sidebands from the experimental results in zero temperature limit (7, 34, 35). However, this limitation is not the major concern of the present study.

When the high-temperature condition characterized by $\beta\hbar\gamma_j < 1$ is assumed for the overdamped Brownian oscillator model, the following hierarchically coupled equations of motion for the reduced density operator can be derived in a nonperturbative manner (18):

$$\frac{\partial}{\partial t}\hat{\sigma}(\mathbf{n},t) = -\left(i\hat{\mathcal{L}}_e + \sum_{j=1}^{N} n_j\gamma_j\right)\hat{\sigma}(\mathbf{n},t) + \sum_{j=1}^{N}\left[\hat{\Phi}_j\hat{\sigma}(\mathbf{n}_{j+},t) + n_j\hat{\Theta}_j\hat{\sigma}(\mathbf{n}_{j-},t)\right], \qquad [6]$$

for sets of nonnegative integers, $\mathbf{n} \equiv (n_1, n_2, \ldots, n_N)$. $\mathbf{n}_{j\pm}$ differs from $\mathbf{n}$ only by changing the specified n_j to $n_j \pm 1$, i.e., $\mathbf{n}_{j\pm} \equiv (n_1, \ldots, n_j \pm 1, \ldots, n_N)$. In Eq. **6**, only the element $\hat{\sigma}(\mathbf{0},t)$ is identical to the reduced density operator $\hat{\rho}(t)$, while the others $\{\hat{\sigma}(\mathbf{n} \neq \mathbf{0},t)\}$ are auxiliary operators to take into account fluctuations in site energies and dissipation of reorganization energies. The Liouvillian corresponding to the electronic Hamiltonian $\hat{H}_e$ is denoted by $\hat{\mathcal{L}}_e$, while the relaxation operators are given by

$$\hat{\Phi}_j = i\hat{V}_j^{\times}, \qquad [7]$$

$$\hat{\Theta}_j = i\left(\frac{2\lambda_j}{\beta\hbar^2}\hat{V}_j^{\times} - i\frac{\lambda_j}{\hbar}\gamma_j\hat{V}_j^{\circ}\right), \qquad [8]$$

where we have introduced the hyper-operator notations, $\hat{O}^{\times}\hat{f} \equiv \hat{O}\hat{f} - \hat{f}\hat{O}$ and $\hat{O}^{\circ}\hat{f} \equiv \hat{O}\hat{f} + \hat{f}\hat{O}$, for any operator $\hat{O}$ and operand $\hat{f}$.

Note that Eq. **6** is a set of equations of motion in the operator form, and hence the numerical results are independent of the representation in which the equations are integrated. The hierarchically coupled equations Eq. **6** continue to infinity, which is impossible to treat computationally. In order to terminate Eq. **6** at a finite stage, we replace Eq. **6** by

$$\frac{\partial}{\partial t}\hat{\sigma}(\mathbf{n},t) = -i\hat{\mathcal{L}}_e\hat{\sigma}(\mathbf{n},t), \qquad [9]$$

for the integers $\mathbf{n} = (n_1, n_2, \ldots, n_N)$ satisfying

$$\mathcal{N} \equiv \sum_{j=1}^{N} n_j \gg \frac{\omega_e}{\min(\gamma_1, \gamma_2, \ldots, \gamma_N)}, \qquad [10]$$

where ω_e is a characteristic frequency for $\hat{\mathcal{L}}_e$ (18). Thus, the required number of the operators $\{\hat{\sigma}(\mathbf{n},t)\}$ is evaluated as $\sum_{k=0}^{\mathcal{N}} \binom{k+N-1}{N-1} = (N+\mathcal{N})!/(N!\mathcal{N}!)$. Note that low-temperature correction terms explained in Appendix should be included into Eq. **6** when the high-temperature condition $\beta\hbar\gamma_j < 1$ is not satisfied.

As demonstrated in ref. 18, the reduced hierarchy equation Eq. **6** can describe quantum coherent wave-like motion, incoherent hopping, and an elusive intermediate EET regime in a unified manner, and reduces to the conventional Redfield and Förster theories in their respective limits of validity. Recently, Jang et al. (15) developed another quantum dynamic equation to interpolate between the Redfield and Förster limits by employing the small polaron transformation (36). The small polaron approach is based on the second-order perturbative truncation with respect to the renormalized electron-phonon coupling, whereas the present hierarchy approach is derived in a non perturbative fashion. It will be interesting to compare the two approaches for future works.

Results and Discussion

In this section, we present and discuss numerical results regarding EET dynamics in the FMO complex of *C. tepidum*. The complex is a trimer made of identical subunits, each containing seven BChls. Because the strongest electronic coupling between two BChls in different FMO monomeric subunit is about an order of magnitude smaller than the local reorganization energies, the coherence between them is rapidly destroyed by the environmental disturbance (26). Therefore, we assume that the intersubunit coupling is vanishingly small and we consider the EET dynamics within one subunit. To simulate the EET dynamics, we use the Hamiltonian

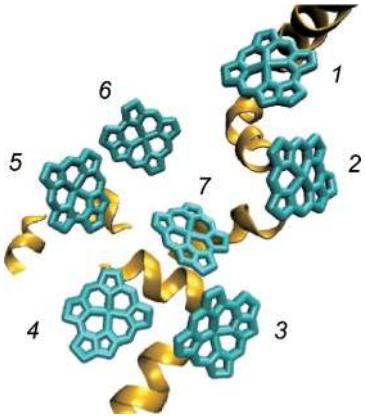

Fig. 1. Seven BChl molecules belonging to the monomeric subunit of the FMO complex. The complex is oriented with BChl 1 and 6 toward the baseplate protein whereas BChl 3 and 4 define the target region in contact with the reaction center complex. The spiral strands are α-helices that are part of protein environment.

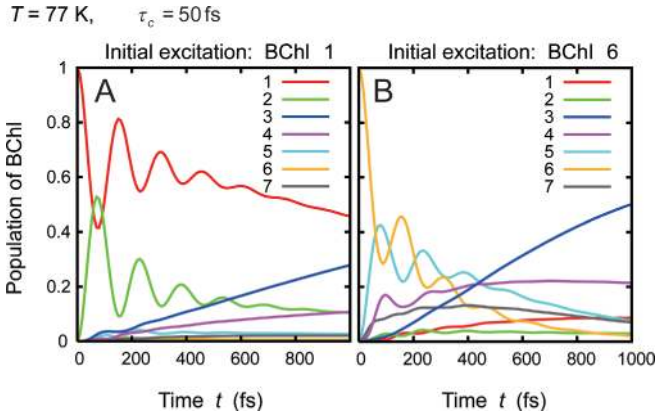

Fig. 2. Time evolution of the population of each BChl in the FMO complex. Calculations were done for cryogenic temperature, $T = 77$ K. The reorganization energy and the phonon relaxation time are set to be $\lambda_j = 35\,\mathrm{cm}^{-1}$ and $\tau_c = \gamma_j^{-1} = 50$ fs, respectively.

for the trimeric structure of the FMO complex given in ref. 26 (supporting information (SI) Table S1.) We use the usual numbering of the BChls, which was originally chosen by Fenna and Matthews (2) (see Fig. 1).

Although the spectral density $\mathcal{J}_j(\omega)$ is a crucial factor to describe EET dynamics, no direct and detailed information on its form is available for the FMO complex at present. Hence, several empirical forms have been employed under the assumption that the spectral densities for the different BChls are equivalent (11, 25–27, 33), and then the phonon relaxation time τ_c estimated by Eqs. **4** and **5** ranges from 35 fs (26)* to 166 fs (25) in the literature. Recently, Read et al. (27) conducted 2D electronic spectroscopic experiments to visualize excitonic structure in the FMO complex of *Prosthecochloris aestuarii*, and they performed simultaneous fitting of the linear and 2D rephasing, nonrephasing, and polarization-dependent spectra by employing the overdamped Brownian oscillator model. To obtain excellent agreement between the experimental data and numerical fitting, they adopted $\lambda_j = 35\,\mathrm{cm}^{-1}$ and $\tau_c = \gamma_j^{-1} = 50$ fs as the values of reorganization energy and relaxation time of the phonons, respectively. Therefore, we also employ these values with the assumption that the phonon spectral densities for the individual BChls are equivalent. For numerical integration of Eq. **6**, the depth of hierarchy we employed here is at most $\mathcal{N} = 12$. For all calculations, the accuracy were checked by changing the values of $\mathcal{N}$ to make sure that the numerical results are converged.

EET Dynamics and Temperature Dependence Following the previous proposal based on theoretical calculations (26), the FMO complex has been assumed to be oriented with BChl 1 and 6 toward the baseplate protein whereas BChls 3 and 4 define the target region in contact with the RC complex. Recently, this orientation was verified experimentally by Wen et al. (5). Accordingly, we adopt BChls 1 or 6 as the initial excited pigment for numerical calculations.

Fig. 2 presents the EET dynamics at cryogenic temperature, $T = 77$ K. These results clearly show that the energy flow in the FMO complex occurs primarily through two EET pathways, which connect spatially proximate and excitonically coupled BChls as demonstrated by Brixner et al. with 2D electronic spectroscopy (11, 25):

* The relaxation function and the symmetrized correlation function at 300 K produced by the spectral density in ref. 26 show nonoscillatory negative values from 80 fs to 1 ps, whose physical origin is not yet clear. Hence, it is impossible to estimate the relaxation time τ_c by employing Eq. **5**. Here, we have estimated the relaxation time only from the initial decay (<80 fs) of the relaxation function.

$$\text{BChls } 1 \rightarrow 2 \rightarrow 3 \rightleftharpoons 4, \qquad \textbf{[11a]}$$

$$\text{BChls } 6 \rightarrow 5, 7, 4 \rightarrow 3. \qquad \textbf{[11b]}$$

The double arrow ($\rightleftharpoons$) in Eq. **11a** indicates that excitation energy equilibrates between BChls 3 and 4 after BChl 3 is populated. In Fig. 2*A*, the long lifetime of BChl 1 is due to the relatively high site energy of BChl 2. Hence, populations of BChls 1 and 3 are dominant at time $t = 1$ ps. In Fig. 2*B*, on the other hand, those of BChls 3 and 4 are dominant at time $t = 1$ ps owing to very fast transport of electronic excitation energy. These behaviors are consistent with the transient pump-probe experiment by Vulto et al. (7, 37) because BChl 1 participates in exciton 3 and BChls 3 and 4 construct exciton 1, where the numbers give the rank starting with the smallest exciton energy. Furthermore, in Fig. 2*A* and *B*, quantum coherent wave-like motions are visible up to 700 fs. This time scale is consistent with the observation by Engel et al. (8) with 2D electronic spectroscopy.

Fig. 3 gives the EET dynamics at physiological temperature, $T = 300$ K. The dynamics at $T = 300$ K is also dominated by the two EET pathways given in Eq. **11**, as described by Adolphs and Renger with the conventional and modified Redfield theories. (26, 38) More noteworthy is that coherent wave-like motions can be clearly observed up to 350 fs even at the physiological temperature. Note that the phonon relaxation time used here, $\tau_c = 50$ fs, was obtained as a numerical fitting parameter for the experimental data; it was not measured directly. For numerical fitting of other 2D spectra of the FMO complex from *C. tepidum* (11), an Ohmic spectral function with an exponential cutoff was employed, i.e., $\mathcal{J}_j(\omega) \propto \lambda_j \omega \exp(-\omega/\omega_c)$ with $\lambda_j = 35\,\text{cm}^{-1}$ and $\omega_c = 50\,\text{cm}^{-1}$ (25), which yields the phonon relaxation time of $\tau_c = 166$ fs. Therefore, attention should be also paid to possibilities of slower phonon relaxation times. Most recently, the present authors have demonstrated that slower phonon relaxation times are preferable in terms of longer lifetime of electronic coherence among pigments (18). Indeed, calculations employing the slower value, $\gamma_j^{-1} = 166$ fs, predict longer-lasting (up to 550 fs) wave-like motions at $T = 300$ K as shown in Fig. 4, which can not be reproduced with conventional Redfield theory because the dynamics are now in the strong non-Markovian regime. In Eq. **6**, slower fluctuations preserve longer-lived quantum coherent oscillation, whereas the Markov approximation in the Redfield theory causes infinitely fast fluctuation and thus collapses the coherence quickly. On the other hand, in the fastest relaxation case in the literature, $\tau_c = 35$ fs (35), numerical results with Eq. **6** also show the wave-like behavior lasting for 350fs at $T = 300$ K, virtually the same as in the case of $\tau_c = 50$ fs.

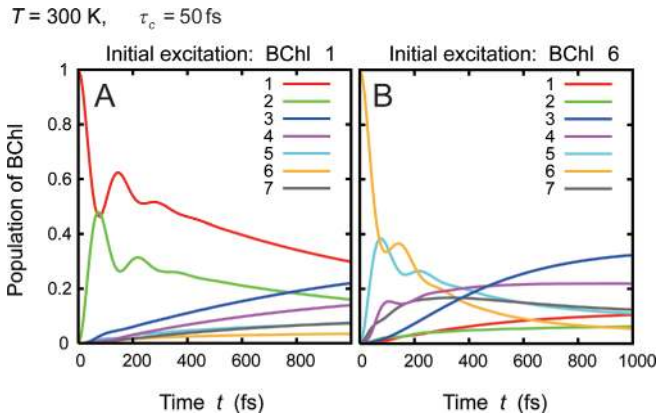

Fig. 3. Time evolution of the population of each BChl in the FMO complex. Calculations were done for physiological temperature, $T = 300$ K. The other parameters are the same as in Fig. 2.

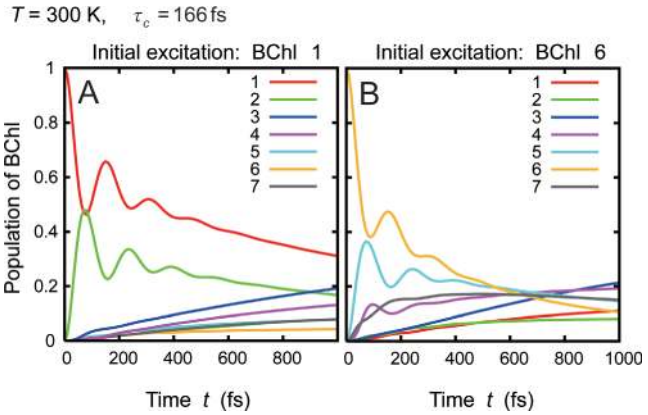

Fig. 4. Time evolution of the population of each BChl in the FMO complex. Calculations were done for the same parameters as in Fig. 3, except for the phonon relaxation times $\tau_c = \gamma_j^{-1} = 166$ fs.

(Fig. S1) Therefore, we expect that long-lived electronic coherence among BChls is present in the FMO complex even at physiological temperatures, irrespective of the phonon relaxation times.

Roles of Quantum Coherence The observation of long-lasting and robust quantum coherence prompts the speculation that quantum effects may play a significant role in achieving the remarkable efficiency of photosynthetic EET. Engel et al. (8) proposed that the FMO complex performs a quantum search algorithm that is more efficient than a classical random walk suggested by the hopping mechanism. Quantum coherence enables the excitation to rapidly and reversibly sample multiple pathways to search for BChl 3 that connects to the RC.

Unidirectional energy flow facilitates the achievement of a near-unity quantum yield. For the unidirectionality, once excitation migrates to the linker pigments between the FMO complex and the RC, it has to be trapped and directed to the RC (27). Here, we explore the idea that the FMO complex may work as a type of "rectifier" for the unidirectional flow from the chlorosome antenna to the RC by taking advantage of quantum coherence and the site energy landscape tuned by the protein scaffold. The basic idea is as follows: If the EET were dominated only by diffusive incoherent hopping, trapping in subsidiary energetic minima would be inevitable. However, quantum delocalization can allow avoidance of the traps to aid the subsequent trapping of excitation by the linker pigments, BChls 3 and 4.

More insight can be gained if attention is given to the site energy of the BChl in the baseplate. It has been reported that the Q_y absorption of the baseplate BChl in *C. tepidum* is located around 800 nm (12, 500 cm^{-1}) (39, 40). This lies between the site energies of BChl 1 (12, 410 cm^{-1}) and BChl 6 (12, 630 cm^{-1}) in ref. 26, and implies that the FMO complex has two windows and their respective onward pathways given in Eq. **11** in order to capture and convey electronic excitation energy from the baseplate without loss. Fig. 5 presents the energy landscapes along the two primary pathways.

In terms of an "energy funnel," it is advantageous that the site energy of BChl 1 is low in comparison to that of the baseplate BChl. Nevertheless, the site energy of BChl 2 is higher than BChl 1, and hence BChl 1 is a local energetic minimum. It is not clear whether there exists a physiological significance to the barrier created by BChl 2. Here, we notice that the energy gap between BChls 1 and 3 is 200 cm^{-1}, which corresponds to the magnitude of thermal energy $k_B T$ at physiological temperature $T = 300$ K. If the BChls in the pathway shown in Fig. 5*A* were arranged in such a way that their site energies monotonically decrease, the relatively flat energy landscape compared to $k_B T$ would allow facile

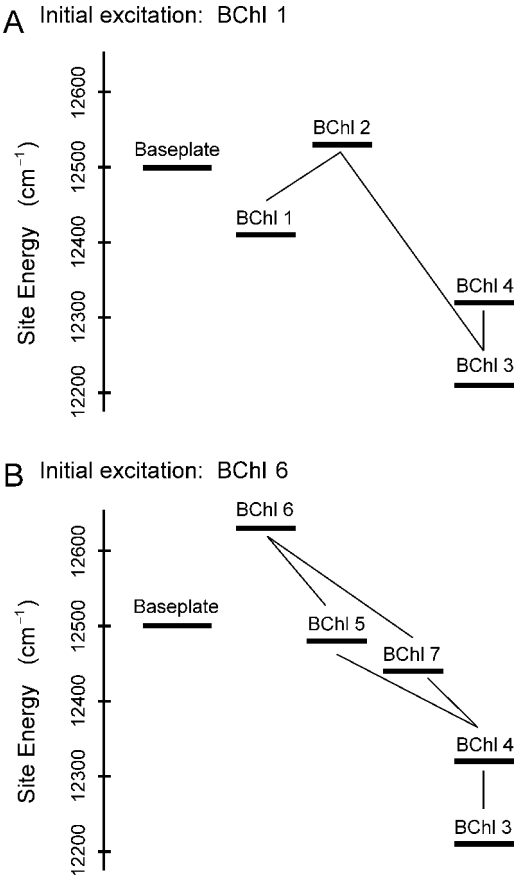

Fig. 5. The energy landscapes along the two primary transfer pathways in the FMO complex: baseplate → BChls 1 → 2 → 3 → 4 (*A*) and baseplate → BChls 6 → 5, 7, 4 → 3 (*B*). The relatively strong couplings between BChls are depicted by solid lines.

backward transfer of excitation away from BChl 3 at physiological temperatures, and the equilibrated population of BChl 3 would decrease. However, the FMO energy landscape is set up such that the site energy of BChl 2 is higher by $\approx 300\,\mathrm{cm}^{-1}$ than that of BChl 3; hence, the back transfer is suppressed and thus BChl 3 is able to have larger amount of population of excitation in equilibrium. (Fig. S2) If the energy transfer from BChl 1 to BChl 2 were a slow incoherent hopping process, the excitation energy would be trapped on BChl 1. However, the wave-like motion induced by the quantum superposition between BChls 1 and 2 enables such trapping to be avoided. Indeed, Figs. 2*A* and 3*A* clearly show that the detrapping of excitation on BChl 1 involves quantum coherent wave-like motion. (Figs. S3 and S4)

The site energy of BChl 6 is higher than the energy of the baseplate BChl. If the deexcitation of the BChl 6 were slow, the excitation could return to the baseplate easily according to the detailed balance condition between BChl 6 and a baseplate BChl. In order to avoid this backward transfer, BChl 6 needs to convey its excitation energy to other BChls as quickly as possible. This is accomplished by having BChl 6 be strongly coupled to both of BChls 5 and 7, which in turn are strongly coupled to BChl 4. Figs. 2, 3, and 4 demonstrate that the initial rises of populations in BChls 5, 7, and 4 are based on quantum wave-like motion irrespective of temperature, and then the excitation of BChl 6 is delocalized coherently over BChls 4, 5, 6, and 7 on the 100-fs time scale. After the ultrafast delocalization, the excitation begins to explore the lowest energy site, BChl 3. This enables the energy flow though the pathway shown in Fig. 5*B* to be unidirectional and highly efficient.

Here, we have not taken into account the effect of static disorder because the suggested standard deviation of the Gaussian distribution of the site energies is $\approx 20\,\mathrm{cm}^{-1}$ (the corresponding fwhm is $\approx 50\,\mathrm{cm}^{-1}$) (25, 27), which is smaller than the site energy gaps in the FMO complex, and therefore the static disorder of the individual sites has little influence on the qualitative nature of the energy landscape. However, even if the static disorder is relatively large, quantum coherence is still expected to help excitation to overcome local energetic traps created by the static disorder as discussed by Renger and Marcus (41) for the variable-range hopping mechanism of electron transfer through DNA.

Concluding Remarks

In this article, we have investigated theoretically the spatial and temporal dynamics of the EET through the FMO complex of *C. tepidum* in order to address the robustness and role of the quantum coherence under physiological conditions. For the description of the dynamics, we applied the hierarchically coupled equations approach, which reduces to the conventional Redfield and Förster theories in their respective limits of validity. The numerical calculations were performed based on the electron-phonon coupling parameters adopted for the fitting of 2D electronic spectroscopic data, where the reorganization energy and the phonon relaxation time are $35\,\mathrm{cm}^{-1}$ and $\tau_c = 50\,\mathrm{fs}$, respectively. The results revealed the presence of quantum coherent wave-like motion persisting for 350 fs even at physiological temperature $T = 300\,\mathrm{K}$. Taking into account the possibility of slower phonon relaxation, we also carried out numerical calculations for $\tau_c = 166\,\mathrm{fs}$. For this case, the dynamic equation used here yields wave-like motion persisting for 550 fs at $T = 300\,\mathrm{K}$, which cannot be reproduced by the conventional Markovian Redfield equation because the dynamics are in the strong non-Markovian regime. Recently, Collini and Scholes (42, 43) showed the presence of a quantum coherent EET process in the conjugated polymer MEH-PPV by means of 2D electronic spectroscopy. Their 2D spectra show that long-lived electronic coherences persist for at least 250 fs after photoexcitation of MEH-PPV in solution at 293 K. Although MEH-PPV is not a photosynthetic complex, their experimental observation of long-lived coherence at room temperature is corroborative for our theoretical predictions. Moreover, as one of potential roles of quantum coherence in the FMO complex, we suggested that quantum coherence allows the FMO complex to work as a rectifier for unidirectional energy flow from the chlorosome antenna to the RC complex. It is reasonable to suppose that quantum coherence can overcome local energetic traps to aid the subsequent trapping of electronic energy by the BChl molecules in contact with the RC complex.

In the present calculations, it has been assumed that the phonon spectral densities for the individual BChls are equivalent and fluctuations in different site energies are uncorrelated. This is because there exists no accurate and detailed information on the coupling between BChls and phonons of the FMO protein. Nevertheless, our results predict the presence of quantum coherence lasting for several hundred femtoseconds at physiological temperature. In the RC complex of a purple bacterium, Groot et al. (44) reported that the phonon relaxation time and electron-phonon coupling strength of one of the BChls are both about 1.5 times different from those of a record BChl in the same complex. Additionally, Lee et al. (14) showed that fluctuations in the bacteriopheophytin and accessory BChl excited energies are strongly correlated enabling long-lasting electronic coherence between them. It has also been reported that correlated fluctuations may enhance the contribution of quantum coherence to EET efficiency of the FMO complex (20). Hence, it is also likely that the couplings between the FMO protein and the embedded BChls are heterogeneous and may be optimized for individual BChl sites in order to preserve longer-lived coherence or to achieve higher efficiency in comparison to the present results. A more detailed understanding of quantum coherent effects in photosynthetic systems demands comprehensive investigations combining

the quantum dynamic theories with quantum chemical calculations and molecular dynamics simulations, in addition to further experimental studies. Investigations from the perspective of quantum information science should also provide insights into the issue.

Appendix: Low-Temperature Correction Terms

For the overdamped Brownian oscillator model of the phonon spectral density, the phonon symmetrized correlation function can be expressed as

$$S_j(t) = \frac{2\lambda_j}{\beta} e^{-\gamma_j t} - \frac{2\lambda_j}{\beta} \sum_{k=1}^{\infty} \frac{2\gamma_j}{\nu_k^2 - \gamma_j^2} \left(\gamma_j e^{-\gamma_j t} - \nu_k e^{-\nu_k t} \right), \qquad \textbf{[A1]}$$

where the first term is the classical correlation function and the second term involving the bosonic Matsubara frequency, $\nu_k \equiv 2\pi k/\beta\hbar$ ($k \geq 1$), represents the quantum corrections. Under the high-temperature condition characterized by $\beta\hbar\gamma_j < 1$, the second term is vanishingly small and then the symmetrized correlation function can be described classically. For low temperature $\beta\hbar\gamma_j > 1$, however, the first term is not sufficient. The quantum dynamic equation based only on the first term does not ensure detailed balance at low temperature; hence, some diagonal elements of the density matrices may be negative.

In this article, we have included only the lowest-order quantum correction involving only $\nu_{k=1}$ to calculate the EET dynamics at $T = 77$K, because the breakdown of the detailed balance condition is minor for the parameters employed here. For the cases of $\gamma_j^{-1} \geq 50$ fs and $T \geq 77$ K, the value of ν_1 is sufficiently large in comparison with γ_j; hence, $\nu_1 \exp(-\nu_1 t)$ can be replaced by Dirac's δ function. As the result, the symmetrized correlation function containing the lowest-order quantum correlation is given by

$$S_j(t) \simeq \frac{2\lambda_j}{\beta} \left(1 - \frac{2\gamma_j}{\nu_1^2 - \gamma_j^2} \gamma_j \right) e^{-\gamma_j t} + \frac{2\lambda_j}{\beta} \frac{2\gamma_j}{\nu_1^2 - \gamma_j^2} \delta(t). \qquad \textbf{[A2]}$$

Following the derivation in ref. 18 with Eq. **A2**, we can obtain a modified equation applicable to the case of $T = 77$ K. The resultant expression can be obtained by the following replacements in Eq. **6**:

$$\hat{\mathcal{L}}_e \to \hat{\mathcal{L}}_e - \sum_{j=1}^{N} \frac{2\lambda_j}{\beta\hbar^2} \frac{2\gamma_j}{\nu_1^2 - \gamma_j^2} \hat{V}_j^{\times} \hat{V}_j^{\times}, \qquad \textbf{[A3]}$$

$$\hat{\Theta}_j \to \hat{\Theta}_j - i \frac{2\lambda_j}{\beta\hbar^2} \frac{2\gamma_j}{\nu_1^2 - \gamma_j^2} \gamma_j \hat{V}_j^{\times}. \qquad \textbf{[A4]}$$

ACKNOWLEDGMENTS. We thank Yuan-Chung Cheng, Tae Kyu Ahn, Thomas Renger, and Alán Aspuru-Guzik for insightful discussions and critical reading of the manuscript. This work was supported by the Director, Office of Science, Office of Basic Energy Sciences, of the U.S. Department of Energy under Contract. DE-AC02-05CH11231 and by the Chemical Sciences, Geosciences and Biosciences Division, Office of Basic Energy Sciences, U.S. Department of Energy under contract DE-AC03-76SF000098. A.I. was supported by Postdoctoral Fellowship for Research Abroad by the Japan Society for the Promotion of Science.

1. Blankenship RE (2002) *Molecular Mechanisms of Photosynthesis.* (World Scientific, London).
2. Fenna RE, Matthews BW (1975) Chlorophyll arrangement in a bacteriochlorophyll protein from *Chlorobium limicola*. *Nature* 258:573–577.
3. Li Y-F, Zhou W, Blankenship RE, Allen JP (1997) Crystal structure of the bacteriochlorophyll a protein from *Chlorobium tepidum*. *J Mol Biol* 271:456–471.
4. Camara-Artigas A, Blankenship RE, Allen JP (2003) The structure of the FMO protein from *Chlorobium tepidum* at 2.2Å resolution. *Photosynth Res* 75:49–55.
5. Wen J, Zhang H, Gross ML, Blankenship RE (2009) Membrane orientation of the FMO antenna protein from *Chlorobaculum tepidum* as determined by mass spectrometry-based footprinting. *Proc Natl Acad Sci USA* 106:6134–6139.
6. Savikhin S, Buck DR, Struve WS (1997) Oscillating anisotropies in a bacteriochlorophyll protein: Evidence for quantum beating between exciton levels. *Chem Phys* 223:303–312.
7. Vulto SIE, et al. (1999) Excited state dynamics in FMO antenna complexes from photosynthetic green sulfur bacteria: A kinetic model. *J Phys Chem B* 103:8153–8161.
8. Engel GS, et al. (2007) Evidence for wavelike energy transfer through quantum coherence in photosynthetic systems. *Nature* 446:782–786.
9. Jonas DM (2003) Two-dimensional femtosecond spectroscopy. *Annu Rev Phys Chem* 54:425–463.
10. Brixner T, Mancăl T, Stiopkin IV, Fleming GR (2004) Phase-stabilized two-dimensional electronic spectroscopy. *J Chem Phys* 121:4221–4236.
11. Brixner T, et al. (2005) Two-dimensional spectroscopy of electronic couplings in photosynthesis. *Nature* 434:625–628.
12. Pisliakov AV, Mancăl T, Fleming GR (2006) Two-dimensional optical three-pulse photon echo spectroscopy. II. Signatures of coherent electronic motion and exciton population transfer in dimer two-dimensional spectra. *J Chem Phys* 124:234505.
13. Cheng Y-C, Fleming GR (2008) Coherence quantum beats in two-dimensional electronic spectroscopy. *J Phys Chem A* 112:4254–4260.
14. Lee H, Cheng Y-C, Fleming GR (2007) Coherence dynamics in photosynthesis: Protein protection of excitonic coherence. *Science* 316:1462–1465.
15. Jang S, Cheng Y-C, Reichman DR, Eaves JD (2008) Theory of coherent resonance energy transfer. *J Chem Phys* 129:101104.
16. Cheng Y-C, Fleming GR (2009) Dynamics of light harvesting in photosynthesis. *Annu Rev Phys Chem* 60:241–262.
17. Ishizaki A, Fleming GR (2009) On the adequacy of the Redfield equation and related approaches to the study of quantum dynamics in electronic energy transfer. *J Chem Phys* 130:234110.
18. Ishizaki A, Fleming GR (2009) Unified treatment of quantum coherent and incoherent hopping dynamics in electronic energy transfer: Reduced hierarchy equations approach. *J Chem Phys* 130:234111.
19. Mohseni M, Rebentrost P, Lloyd S, Aspuru-Guzik A (2008) Environment-assisted quantum walks in photosynthetic energy transfer. *J Chem Phys* 129:174106.
20. Rebentrost P, Mohseni M, Aspuru-Guzik A (2009) Role of quantum coherence in chromophoric energy transport. *J Phys Chem B* 113:9942–9947.
21. Rebentrost P, Mohseni M, Kassal I, Lloyd S, Aspuru-Guzik, A (2009) Environment-assisted quantum transport. *New J Phys* 11:033003.
22. Plenio MB, Huelga SF (2008) Dephasing-assisted transport: quantum networks and biomolecules. *New J Phys* 10:113019.
23. Förster T (1948) Zwischenmolekulare energiewanderung und fluoreszenz. *Ann Phys* 2:55–75.
24. Redfield AG (1957) On the theory of relaxation processes. *IBM J Res Dev* 1:19–31.
25. Cho M, Vaswani HM, Brixner T, Stenger J, Fleming GR (2005) Exciton analysis in 2D electronic spectroscopy. *J Phys Chem B* 109:10542–10556.
26. Adolphs J, Renger T (2006) How proteins trigger excitation energy transfer in the FMO complex of green sulfur bacteria. *Biophys J* 91:2778–2797.
27. Read EL, et al. (2008) Visualization of excitonic structure in the Fenna-Matthews-Olson photosynthetic complex by polarization-dependent two-dimensional electronic spectroscopy. *Biophys J* 95:847–856.
28. Tanimura Y (2006) Stochastic Lioville, Langevin, Fokker-Planck, and master equation approaches to quantum dissipative systems. *J Phys Soc Jpn* 75:082001.
29. Grabert H, Schramm P, Ingold G-L (1988) Quantum Brownian motion: The functional integral approach. *Phys Rep* 168:115–207.
30. Fleming GR, Cho M (1996) Chromophore-solvent dynamics. *Annu Rev Phys Chem* 47:109–134.
31. Kubo R (1963) Stochastic Liouville equations. *J Math Phys* 4:174–183.
32. Zigmantas D, et al. (2006) Two-dimensional electronic spectroscopy of the B800-B820 light-harvesting complex. *Proc Natl Acad Sci USA* 103:12672–12677.
33. Read EL, et al. (2007) Cross-peak-specific two-dimensional electronic spectroscopy. *Proc Natl Acad Sci USA* 104:14203–14208.
34. Wendling M, et al. (2000) Electron-Vibrational coupling in the Fenna-Matthews-Olson complex of *Prosthecochloris aestuarii* determined by temperature-dependent absorption and fluorescence line-narrowing measurements. *J Phys Chem B* 104:5825–5831.
35. Renger T, Marcus RA (2002) On the relation of protein dynamics and exciton relaxation in pigment-protein complexes: An estimation of the spectral density and a theory for the calculation of optical spectra. *J Chem Phys* 116:9997–10019.
36. Rackovsky S, Silbey R (1973) Electronic-energy transfer in impure solids. I. Two molecules embedded in a lattice. *Mol Phys* 25:61–72.
37. Vulto SIE, et al. (1998) Excited-state structure and dynamics in FMO antenna complexes from photosynthetic green sulfur bacteria. *J Phys Chem B* 102:10630–10635.
38. Müh F, et al. (2007) α-Helices direct excitation energy flow in the Fenna-Matthews-Olson protein. *Proc Natl Acad Sci USA* 104:16862–16867.
39. Francke C, Amesz J (1997) Isolation and pigment composition of the antenna system of four species of green sulfur bacteria. *Photosynth Res* 52:137–146.
40. Frigaard N-U, et al. (2005) Isolation and characterization of carotenosomes from a bacteriochlorophyll *c*-less mutant of *Chlorobium tepidum*. *Photosynth Res* 86:101–111.
41. Renger T, Marcus RA (2003) Variable-range hopping electron transfer through disordered bridge states: Application to DNA. *J Phys Chem A* 107:8404–8419.
42. Collini E, Scholes GD (2009) Coherent intrachain energy migration in a conjugated polymer at room temperature. *Science* 323:369–373.
43. Collini E, Scholes GD (2009) Electronic and vibrational coherences in resonance energy transfer along MEH-PPV chains at room temperature. *J Phys Chem A* 113:4223–4241.
44. Groot ML, Yu JY, Agarwal R, Norris JR, Fleming GR (1998) Three-pulse photon echo measurements on the accessory pigments in the reaction center of *Rhodobacter sphaeroides*. *J Phys Chem B* 102:5923–5931.